钟罩型电子束焊接接头的疲劳寿命分析

杨 波[1], 杨新华[1], 付 玮[1], 胡树兵[2], 肖建中[2]
(1. 华中科技大学 土木工程与力学学院, 武汉 430074
2. 华中科技大学 材料科学与工程学院, 武汉 430074)

摘 要: 利用 MSC公司的系列软件, 模拟试验加载条件, 将 TC4钛合金钟罩型电子束焊接试件划分成焊缝、热影响区和母材 3个区域, 同时考虑热影响区材料强度的梯度分布, 建立有限元模型, 详细分析了焊件中的应力和疲劳寿命分布, 沿不同观察路径考察了应力分布的规律, 并将疲劳寿命分析结果与试验结果进行了比较. 结果表明, 焊缝对焊件的受力分布有明显影响, 并导致应力在焊趾处集中, 应力集中系数约为 1.3, 应力集中造成焊件寿命分布不均, 从而降低了焊件的疲劳寿命; 焊趾附近为低疲劳寿命区域, 疲劳破坏容易从焊趾处起源.

关键词: TC4钛合金; 电子束焊接; 钟罩型焊接接头; 疲劳寿命
中图分类号: TG115.28 文献标识码: A 文章编号: 0253-360X(2011)05-0069-04

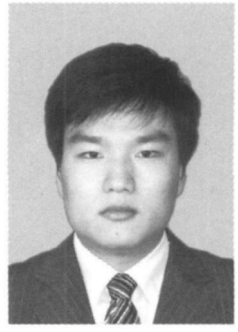

杨 波

0 序 言

目前, 针对钛合金电子束焊接的研究多数采用试验测试和观察的方法. 李晓延等人[1]研究了 TC4钛合金薄板激光焊和电子束焊接头的疲劳性能, 测试了不同应力水平下的疲劳寿命. 许鸿吉等人[2]通过室温拉伸、室温缺口拉伸、显微硬度以及金相分析研究了 TC4钛合金电子束焊接接头的显微组织和性能. 左景辉等人[3]采用超声波疲劳试验确定了 TC4钛合金双态和网篮两种组织的疲劳寿命(S-N)曲线, 并观察了疲劳断口形貌特征.

随着计算机技术和计算仿真软件的发展, 利用有限元软件研究钛合金焊接性能开始受到重视. 陈芙蓉等人[4]采用 ANSYS有限元软件对 TC4钛合金电子束焊接温度场以及焊接接头应力场的变化和残余应力分布进行了数值模拟, 研究了焊后电子束局部热处理工艺对焊接接头残余应力的影响规律. 文中将 TC4钛合金钟罩型电子束焊接试件划分成焊缝、热影响区和母材 3个区域, 同时考虑热影响区材料强度的梯度分布, 采用 MSC公司的系列软件, 在应力分析的基础上进一步开展了焊件的疲劳寿命分析, 并与试验结果进行比较. 有关这方面的工作, 尚未见有文献报道.

收稿日期: 2010-03-01
基金项目: 国防 973项目(61362)

1 钟罩型焊缝的有限元模型

1.1 几何模型

电子束焊接的工艺参数主要有聚焦电流、电子束流和焊接速度. 通过调节聚焦电流改变电子束的焦点、调节电子束流的大小以及焊接速度等能够形成不同形状的焊缝. 钟罩型焊缝是常见的一种焊缝形式. 计算中, 焊件模型采用 200 mm×90 mm×20 mm的长方体, 焊接沿长度方向, 并与轧制方向垂直.

此处利用问题的对称性, 取焊件的四分之一建立有限元模型. 在焊接过程中, 熔凝区两侧一定区域的母材也会受到焊接高温的影响, 但是母材并未熔化, 只是金相组织和力学性能发生一定变化, 称为热影响区. 热影响区的力学性能与母材不同, 一般介于焊缝和母材之间, 并且呈现梯度分布的特征. 为建模方便, 假设单侧热影响区的厚度为相同高度处焊缝熔宽的 0.15倍, 将热影响区划分为 3层, 并按由母材到焊缝的方向分别称为 1区、2区和 3区, 每层厚度相同, 如图 1所示. 模型采用六面体单元进行网格划分, 单元边长为 0.8 mm. 模型共包含 121 024个节点, 95 580个单元.

1.2 模型材料

采用理想弹塑性材料模型. 假设钛合金母材、1.2 3三层热影响区和焊缝的屈服极限和强度极限呈线性递减关系, 不同区域的材料属性见表 1.

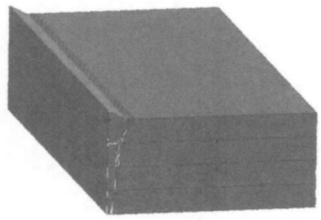

图 1 焊件几何模型

Fig. 1 Geometrical model of weldment

表 1 不同计算区域采用的材料属性

Table 1 Material properties in different computational regions of weldment

	弹性模量 E/GPa	泊松比 μ	屈服强度 R_{eL}/MPa	抗拉强度 R_m/MPa
母材	114	0.3	830	887
1区	114	0.3	820	880
2区	114	0.3	810	870
3区	114	0.3	800	860
焊缝	114	0.3	790	850

1.3 载荷边界条件

焊件疲劳试验的最大应力为 588 MPa,应力比 R=0.1,载荷为正弦波,频率为 10 Hz. 在模型对称面上施加对称约束边界条件,端部截面施加 x, y两个方向的位移约束和 x方向的拉应力.

2 应力计算及结果

在焊件两端施加 588 MPa的拉应力,利用 MSC. NASTRAN软件进行分析,得到模型的 Mises应力云图,见图 2. 可以看出,由于模型比较规则,焊件内部应力基本处于 500~600 MPa水平,最大应力发生在焊缝余高与母材的交汇(即焊趾)处,并且沿长度方向,整条焊缝余高与母材的交汇处都处于高应力区域. 最小应力发生在焊缝余高的顶端.很明显,焊件的应力受到了焊缝的影响.

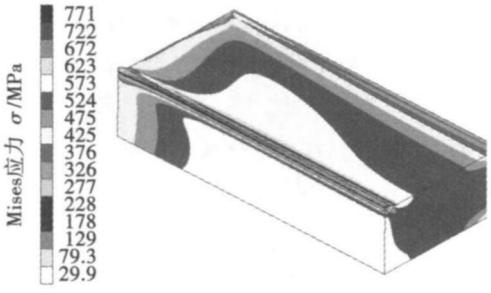

图 2 Mises应力云图

Fig. 2 Contour of Mises stress

为了更加直观地反映分析结果,在模型上选取 9条不同路径,见图 3,绘出应力在这些路径上的变化趋势. 图 4为沿不同路径的应力变化曲线.

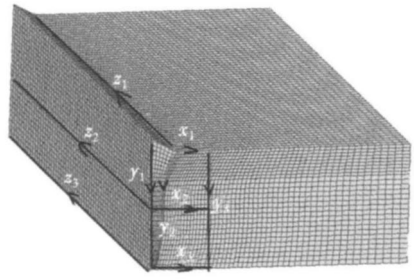

图 3 应力分布的观察路径

Fig. 3 Paths used for observing stress distributions

在图 4a中,焊件沿 x方向的拉应力最大,占主导地位,焊缝余高顶部约 32 MPa,沿 x方向迅速升高并在焊缝余高与母材交界处附近达到 810 MPa的最大值,之后有所降低,并稳定在 630 MPa左右. 焊缝对焊件的受力分布有明显影响,并导致应力集中,应力集中系数约为 1.3. 比较图 4b, c可以发现,焊件在 x_2和 x_3路径上的应力分布曲线基本相同, Mises应力维持在 580 MPa左右, x方向应力维持在 620~630 MPa左右,两者皆呈缓慢下降趋势. y方向应力由压应力逐渐转变为拉应力,应力值维持在 10 MPa以内,并缓慢上升. z方向应力维持在 110 MPa附近,同样有缓慢上升的趋势. 图 4d为焊件沿 y_1路径的应力分布. 由焊缝余高顶端至焊缝底部, Mises等效应力先是逐渐增大,达到一定水平后,基本保持不变. 焊缝余高顶端 Mises等效应力为 83 MPa,当 y坐标小于 -3 mm时, Mises等效应力基本保持在 590 MPa左右. 由于 x方向的应力占主导地位, x方向的应力趋势与 Mises等效应力基本保持一致. 当 y方向坐标在 +2~-8 mm之间时,焊件承受 y方向的压应力. 在 z方向上,焊件先承受压应力,再逐渐转变为拉应力并保持在 110 MPa左右. 图 4e为焊件沿 y_2路径的应力分布. 在焊缝余高附近的区域应力变化较大,当远离焊缝余高时,各个应力都维持在一定水平. 在 y_2路径的上端,由于靠近焊缝余高与母材交界处的应力集中区域,因此 Mises等效应力达到了较高的水平. 随着 y坐标的减小, Mises等效应力迅速下降. 可以看出,由于焊缝余高所受应力较小,而其周围的应力较大,并且焊缝余高边缘紧邻着应力集中区域,所以从焊缝余高的下部向母材方向延伸,出现一个半岛区域,该区域的应力比周围母材的应力低. y_2路径上经过半岛区域的地

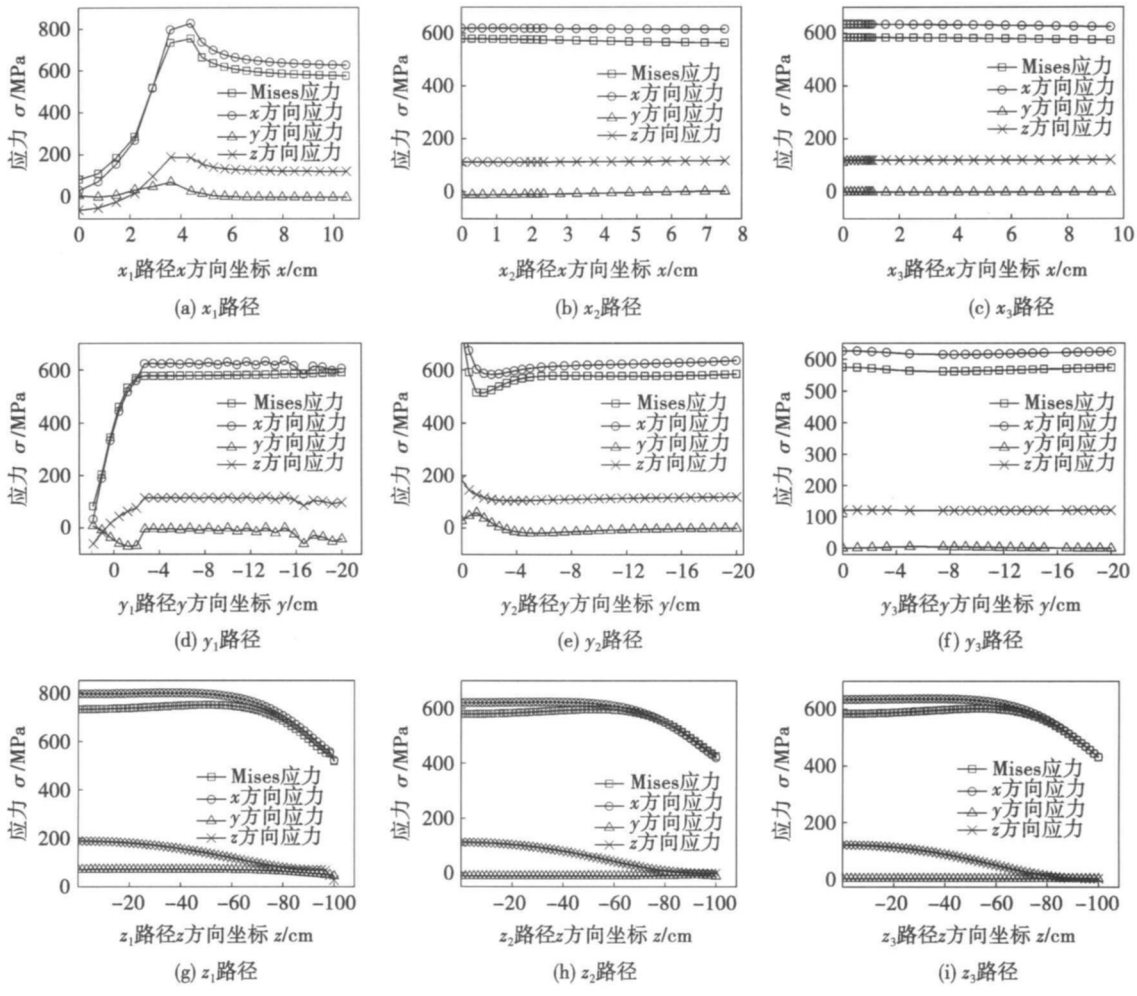

图 4　沿不同路径的应力曲线

Fig. 4　Stress curves along different paths

方应力明显下降,之后回升到 580 MPa左右并保持持平. 从中可以得出焊缝余高对模型应力分布影响很大的结论. 图 4 为焊件沿 y_3 路径的应力分布. 可以看出,在远离焊缝的母材区域,不同应力分量基本保持不变. 图 4(g)~图 4(i)分别为焊件沿 z_1, z_2 和 z_3 路径的应力分布. 在 3条路径上模型所受应力都在靠近模型中部时维持在一定的水平,当接近模型端部时开始下降. z_1路径为焊缝余高与母材的交界处,整体 Mises等效应力都处于很高的水平,达到 730 MPa以上,这也是疲劳裂纹最容易发生的区域.

3　疲劳计算及结果

3.1　材料的 S—N曲线

图 5为试验测得的 TC4钛合金母材和焊接接头的 S—N曲线[1]. 可以看出, TC4钛合金高能束流焊接接头的疲劳寿命在高应力水平和较低的应力水平时不同. 当接头在高应力水平服役时,疲劳寿命明显低于母材的疲劳寿命,但在较低的应力水平时,焊接接头的疲劳寿命可能高于母材的疲劳寿命.

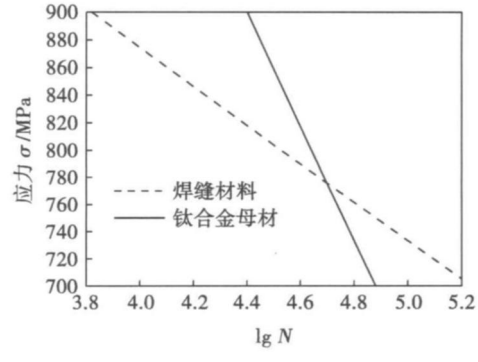

图 5　TC4钛合金母材和焊接接头的 S—N曲线

Fig. 5　S—N curves for TC4 base metal and welding seam

根据上述 S—N曲线,确定母材和焊接接头的材料参数. 母材 $m=4.399\,6$, $\lg C=17.397\,3$;焊缝 $m=8.157\,7$, $\lg C=28.249\,5$. 3个热影响区由于抗

拉强度各不相同，S－N曲线也存在一定差异.

3.2 载荷历程

根据前述的载荷条件，创建载荷历程，如图 6 所示.

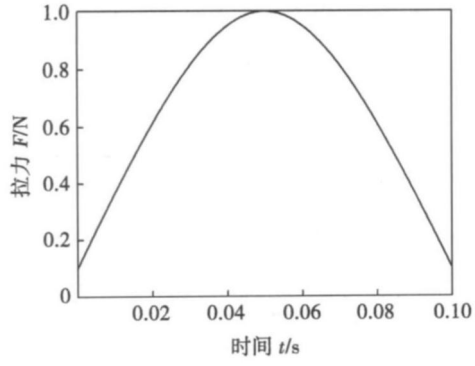

图 6 载荷历程

Fig. 6 Loading history

3.3 疲劳寿命计算结果

利用 MSC. FATIGUE软件进行计算，获得如图 7 所示的焊件疲劳寿命分布云图. 从图 7中可以看出焊趾顶部以及热影响区为模型最容易发生破坏的区域，最低寿命为 89 078周次. 由于焊缝余高的存在，焊趾顶部会出现较大的应力集中，同时热影响区顶部受焊趾顶部应力集中的影响，也出现较高水平的应力，从而导致其疲劳寿命较低. 计算所得焊缝区域的疲劳寿命高出母材很多，达到 8.3×10^5 周次以上，这是因为计算中没有考虑焊接缺陷. 通常，焊缝在凝固过程中会产生气孔，这些孔洞对焊缝的承载能力以及疲劳寿命有较大影响，在孔洞附近会产生应力集中，形成较大的应力，从而降低焊缝疲劳寿命. 在 25 Hz应力比 R=0.1，最大应力约 588 MPa (即 0.65 R_m)的三角波循环载荷作用条件下对 TC4

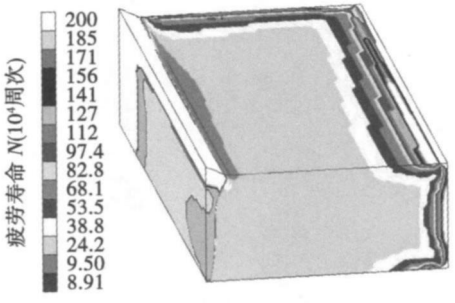

图 7 疲劳寿命分布云图

Fig. 7 Distribution contours of fatigue life

钛合金焊接接头进行疲劳寿命试验，两个试件的疲劳寿命分别为 98 139周次和 105 537周次[1]. 可以看出，计算结果比试验结果偏小，但和试验非常接近.

4 结 论

(1) 由于加载的原因，焊件沿 x方向的拉应力占主导地位，但焊缝对焊件的应力分布有明显影响.

(2) 在焊缝余高顶部 x方向的拉应力最小，沿着 x方向远离焊缝中心，则应力迅速升高，并在焊缝余高与母材交界 (即焊趾)附近达到最大值，之后出现一定程度的下降.

(3) 焊趾处的应力集中系数约为 1.3，由焊缝余高引起的应力集中造成焊件疲劳寿命的分布不均匀，从而降低了焊件的疲劳寿命，疲劳破坏容易从应力集中比较严重的焊趾顶部起源.

参考文献：

[1] 李晓延，巩水利，陈 俐. TC4钛合金薄板高能束焊接接头疲劳性能研究[J]. 航空材料学报，2005，25(4)：26－29.
Li Xiaoyan，Gong Shuili，Chen Li. A study of fatigue life of TC4 titanium alloy sheet and its high density beams welded joints[J]. Journal of Aeronautical Materials，2005，25(4)：26－29.

[2] 许鸿吉，尹丽香，李晋炜，等. TC4钛合金电子束焊接接头组织和性能[J]. 焊接学报，2005，26(11)：43－46.
Xu Hongji，Yin Lixiang，Li Jinwei，et al. Microstructures and properties of TC4 alloy joints welded by the electron beam welding[J]. Transactions of the China Welding Institution，2005，26(11)：43－46.

[3] 左景辉，王中光，韩恩厚. Ti-6Al-4V合金的超高周疲劳行为[J]. 金属学报，2007，43(7)：705－709.
Zuo Jinghui，Wang Zhongguang，Han Enhou. Ultra-high cycle fatigue behavior of Ti-6Al-4V alloy[J]. Acta Metallurgica Sinica，2007，43(7)：705－709.

[4] 陈芙蓉，解瑞军，张可荣. TC4钛合金焊后电子束局部热处理残余应力有限元分析[J]. 内蒙古工业大学学报，2006，25(1)：21－24.
Chen Furong，Xie Ruijun，Zhang Kerong. Finite element analysis of residual stresses in TC4 titanium alloy after post-weld electron beam local heat treatment[J]. Journal of Inner Mongolia University of Technology，2006，25(1)：21－24.

作者简介：杨 波，男，1985年出生，硕士. 主要从事钛合金电子束焊接技术的研究. Email：yangxinh@263.net

通讯作者：杨新华，男，教授，博士研究生导师. Email：yangxinh@263.net

tic stress concentration

Microstructures and solderability of SnCuNixPr lead-free solder LUO Jiadong, XUE Songbai, ZENG Guang, HU Yuhua (School of Materials Science and Technology, Nanjing University of Aeronautics and Astronautics, Nanjing 210016, China). p. 57—60

Abstract: Effects of rare earth element Pr on the wetting performance, mechanical properties and microstructures of Sn0.7Cu0.05Ni lead-free solder were studied. The inherent relationship between the microstructures and properties of the solder was preliminarily discussed. The experimental results show that the suitable amount of Pr addition is 0.025%-0.075%, and the most appropriate amount is 0.05%, at which composition the solder exhibits the best wetting performance and mechanical properties. The surface tension of the liquid solder was significantly reduced due to the addition of rare earth Pr and the wetting performance was improved. The microstructures of the soldered joints were evidently refined, which resulted from the pinning effect on the grain boundaries migration due to the addition Pr, and the shear strength was improved obviously. It was also found that the activity of the rare earth element of Pr may be reduced because of excessive oxidation and the enlargement of the comprehensive effect of stress field caused by excessive addition of Pr.

Key words: Pb-free solder; rare earth element Pr; wetting performance; mechanical properties; microstructure

Analysis on continuous cooling transformation curves of simulated heat affected zone for SA508-3 steel in nuclear power CHI Luxin[1,2], MA Yonglin[2], XING Shuqing[2], ZHAO Yongtao[2], CHEN Furong[2], CHEN Zhongyi[2] (1. School of Materials Science and Engineering, Inner Mongolia University of Technology, Huhhot 010051, China; 2. School of Material and Metallurgy, Inner Mongolia University of Science and Technology, Baotou 014010, China). p. 61—64

Abstract: The SA508-3 steel used in nuclear power was used to determine continuous cooling transformation (SH-CCT) diagram of simulated heat affected zone (HAZ) by thermal expansion method on Gleeble 1500D thermal simulation testing machine, and the microstructure characteristics of HAZ at $t_{8/5}$ from 3.75 s to 20 000 s were investigated. It was found that the microstructures were changed much from the base metal because of the influence of the cooling time ($t_{8/5}$). When the $t_{8/5}$ is less than 15 s, the phase transformation to obtain all martensite happens, the cooling time range to get all the bainite is from 60 s to 3 000 s, and if all the ferrite and pearlite can be obtained if the $t_{8/5}$ is more than 6 000 s. The hardness of HAZ is higher than 350 HV and there are harden quenching tendency and the crack sensitivity when the $t_{8/5}$ is less than 100 s, softening phenomena easily happens and the hardness of HAZ is lower than that of the base metal when the $t_{8/5}$ is more than 20 000 s. The cold cracking can be avoided only at the proper preheating temperature.

Key words: SA508-3 steel; cooling rate; continuous cooling transformation curves; crack sensitivity

Effect of content of Ag on physical properties and solderability of Sn0.7Cu solder ZHAO Kuaile, YAN Yanfu, TANG Kun, SHENG Yangyang (School of Materials Science & Engineering, Henan University of Science & Technology, Luoyang 471003, China). p. 65—68

Abstract: SnCu eutectic solder is considered as the most potential substitutes of SnPb solder, particularly in wave soldering. But compared to other lead-free solders, its poor physical properties and spreading peformance limits its wide application. A new solder is made by adding trace Ag into Sn0.7Cu alloy to improve its performance. The results show that content of Ag has little influence on the melting point of Sn0.7CuxAg solder. The melting point of Sn0.7Cu0.2Ag is higher only 0.3 ℃ than that of matrix solder. The resistivity increases with the increase of the content of Ag. At the same time, the spreading performance of the new solder is improved by adding trace Ag into Sn0.7Cu. The spreading area of Sn0.7Cu0.2Ag reaches the maximum value of 28.61 mm^2 and is increased 25.5% than that of the matrix solder, which is mainly related to the formation of the rich Ag phase and the thickness and shape of the metal intermetallic compound between the solder and the substrate.

Key words: eutectic solder; melting point; resistivity; spreading area

Analysis of fatigue life of electron beam welding seam with bell shape YANG Bo[1], YANG Xinhua[1], FU Wei[1], HU Shubing[2], XIAO Jianzhong[2] (1. School of Civil Engineering and Mechanics, Huazhong University of Science and Technology, Wuhan 430074, China; 2. School of Materials Science and Engineering, Huazhong University of Science and Technology, Wuhan 430074, China). p. 69—72

Abstract: The bell-shaped TC4 titanium alloy joint of electron beam welding were divided into three zones, namely weld seam, heat affected zone and base metal. Considering the gradient distribution of the material strength in the heat affected zone, the finite element model was founded. The series of software of MSC company were used to analyze the distribution of stress and fatigue life under the simulated experimental loading conditions, and the stress distribution along different paths were investigated, and the simulating results of fatigue life were compared with that of experiments. It is shown that the weld seam has noticeable effect on stress distribution of the weldment, which causes the stress concentration with the stress concentration factor of about 1.3 at the weld toe. The uneven distribution of weldment life is caused by stress concentration, so that the fatigue life of weldment is reduced. The fatigue failure usually starts at the weld toe.

Key words: TC4 titanium alloy; electron beam welding; bell-shaped weld seam; fatigue life

Microstructure and properties of TiC$_p$/Al composite coating by argon arc cladding MENG Junsheng, SHI Xiaoping, WANG Zhenting, WANG Yongdong (School of Materials Science and Engineering, Heilongjiang Institute of Science and Technology, Harbin 150027, China). p. 73—76

Abstract: By using argon arc cladding, TiC$_p$/Al composites coating was in-situ synthesized on the ZL104 alloy surface. The microstructures and properties of the composites coatings were investigated by X-ray diffractometer, scanning electron microscope and microhardness tester. The results show that if the content of (Ti+C) is less than 30% during argon arc cladding, both TiC particle and Al$_3$Ti compounds can be found. If the con-